Time-Scale Analysis of Motor Unit Action Potentials

Constantinos S. Pattichis,* *Member, IEEE,* and Marios S. Pattichis, *Associate Member, IEEE*

***Abstract*— Quantitative analysis in clinical electromyography (EMG) is very desirable because it allows a more standardized, sensitive and specific evaluation of the neurophysiological findings, especially for the assessment of neuromuscular disorders. Following the recent development of computer-aided EMG equipment, different methodologies in the time domain and frequency domain have been followed for quantitative analysis. In this study, the usefulness of the wavelet transform (WT), that provides a linear time-scale representation is investigated, for describing motor unit action potential (MUAP) morphology. The motivation behind the use of the WT is that it provides localized statistical measures (the scalogram) for nonstationary signal analysis. The following four WT's were investigated in analyzing a total of 800 MUAP's recorded from 12 normal subjects, 15 subjects suffering with motor neuron disease, and 13 from myopathy: Daubechies with four and 20 coefficients, Chui (CH), and Battle–Lemarie (BL). The results are summarized as follows: 1) most of the energy of the MUAP signal is distributed among a small number of well-localized (in time) WT coefficients in the region of the main spike, 2) for MUAP signals, we look to the low-frequency coefficients for capturing the average waveshape of the MUAP signal over long durations, and we look to the high-frequency coefficients for locating MUAP spike changes, 3) the Daubechies 4 wavelet, is effective in tracking the transient components of the MUAP signal, 4) the linear spline CH (semiorthogonal) wavelet provides the best MUAP signal approximation by capturing most of the energy in the lowest resolution approximation coefficients, and 5) neural network DY (DY) of Daubechies 4 and BL WT coefficients was in the region of 66%, whereas DY for the empirically determined time domain feature set was 78%. In conclusion, wavelet analysis provides a new way in describing MUAP morphology in the time-frequency plane. This method allows for the fast extraction of localized frequency components, which when combined with time domain analysis into a modular neural network decision support system enhances further the DY to 82.5% aiding the neurophysiologist in the early and accurate diagnosis of neuromuscular disorders.**

***Index Terms*— Electromyography (EMG), motor unit action potentials (MUAP's), time-scale analysis, wavelet analysis.**

I. Introduction

STRUCTURAL reorganization of the motor unit, the smallest functional unit of muscle, takes place because of disorders affecting peripheral nerve and muscle. Motor unit morphology can be studied by recording its electrical activity, the procedure known as electromyography (EMG). In clinical EMG motor unit action potentials (MUAP's) are recorded using a needle electrode at slight voluntary contraction. The MUAP reflects the electrical activity of a single anatomical motor unit. It represents the compound action potential of those muscle fibers within the recording range of the electrode. Features of MUAP's extracted in the time domain such as duration, amplitude, and phases proved to be very valuable in differentiating between muscle and nerve diseases [1] with the duration measure being the key parameter used in clinical practice. However, the measurement of the duration parameter is a difficult task depending on the neurophysiologist and/or the computer-aided method used. The definition of widely accepted criteria that will allow the computer-aided measurement of this parameter are still lacking [2]. On the other hand, frequency domain features of MUAP's like the mean, or median frequency, bandwidth, and quality factor provide additional information in the assessment of neuromuscular disorders and it has recently been shown that the discriminative power of the MUAP mean or median frequency is comparable to the duration measure [3] or the spike duration measure [4]. Furthermore, earlier EMG frequency analysis studies showed a displacement toward lower frequencies for neurogenic lesions, with the opposite being true for myogenic lesions [5]–[9]. These findings were also confirmed by Larsson and coworkers [10], [11] who devised a method for the automated measurement of the EMG power content of four octave band filters with center frequencies at 50, 200, 800, and 1600 Hz. Even though frequency-domain techniques describe the frequencies present in the signal, information about their occurrence in time is missing. The objective of this paper is to investigate the analysis of MUAP signal characteristics in both the time and frequency domains using the wavelet transform (WT). The usefulness of wavelet analysis in EMG data was presented in a recent pilot study by our group [12].

In this study four different wavelets were investigated: Daubechies with four (DAU4) and 20 (DAU20) coefficients [13], Chui (CH) [14] and Battle–Lemarie (BL) [15]. The main characteristics of these wavelets which motivated their application on MUAP analysis are outlined below.

1) The orthogonal WT decomposes a signal into a set of orthogonal basis functions. Unlike the short time Fourier transform (STFT) which uses orthogonal sinusoids over the window, while the basis functions from overlapping windows are not orthogonal, the WT basis functions are always orthogonal. This means that every WT coefficient represents an entirely different signal component.
2) Assuming that high frequencies change rapidly, while low frequencies change slowly, the WT uses long

Manuscript received December 5, 1997; revised May 7, 1999. This work was supported in part by the Cyprus Institute of Neurology and Genetics. *Asterisk indicates corresponding author.*

*C. S. Pattichis is with the Department of Computer Science, University of Cyprus, Kallipoleos 75, P.O. Box 537, CY-1678, Nicosia, Cyprus (e-mail: pattichi@ucy.ac.cy).

M. S. Pattichis is with the Department of Electrical and Computer Engineering, University of New Mexico, Albuquerque, NM 87131-1356 USA (e-mail: pattichis@eece.unm.edu).

Publisher Item Identifier S 0018-9294(99)07641-7.

duration windows for capturing the low-frequency components and short duration windows for capturing the high-frequency components. This means that for MUAP signals we look at the high-frequency coefficients for locating abrupt signal changes, while we look at the low-frequency coefficients for capturing the average behavior of the signal over long durations. In contrast, the STFT uses a fixed window and does not provide a varying time-frequency resolution. (For the STFT, the use of a short window results in low spectral resolution, whereas the use of a longer window improves the-frequency resolution but results in a loss of time-resolution.)

3) For the case of the DAU4, the WT coefficients at the highest-frequency scales provide high time-resolution of only four signal samples. This allows the DAU4 wavelet to effectively track the MUAP main spike transient signal at a time resolution that the STFT simply cannot match.
4) The energy in the MUAP signal is distributed among a small number of well localized in time WT coefficients. In addition to the time-frequency features, the WT supports multiresolution analysis of the MUAP signals. Briefly, at each stage (scale) the WT provides two sets of coefficients: the scaling function coefficients, and the wavelet function coefficients. Each successive stage replaces the scaling function coefficients by another two sets of scaling function and wavelet coefficients. In terms of analyzing MUAP signals, we compare the difference between the two sets of scaling function coefficients, coming from successive scales, to recognize the signal features that the set of wavelet coefficients represents.

Wavelet analysis was carried out on MUAP's recorded from normal subjects and subjects suffering with motor neuron disease and myopathy. The performance of wavelet analysis is compared to traditional time and frequency analysis. In the next section, wavelet analysis is briefly introduced, and the advantages and disadvantages of the four wavelets investigated are discussed. In Sections III and IV, EMG experimental procedure and material are given, respectively. Results are described in Section V and discussion is presented in Section VI.

II. Wavelet Analysis

A. The Wavelet Transform

In this section, the WT is presented as a time-scale analysis tool [16]. Along with the algorithm, we analyze the relationship between the wavelet coefficients and the time-frequency plane. The WT algorithm consists of the decomposition and the reconstruction phases. For our purposes, we focus on describing the decomposition phase. In the decomposition phase the original signal x is decomposed into its high-frequency and low-frequency components [see Fig. 1(a)]. The original discrete signal $x_0, x_1, x_2, \ldots$ is lowpass filtered by $h_0, h_1, h_2, \ldots$ and downsampled by two to produce the low-frequency component signal (smooth signal) $s_0^{-1}, s_1^{-1}, s_2^{-1}, \ldots$. Similarly, the original discrete signal is highpass filtered by $g_0, g_1, g_2, \ldots$ and downsampled by two to produce the high-frequency content signal (detail signal) $d_0^{-1}, d_1^{-1}, d_2^{-1}, \ldots$. In our notation, the superscript -1 of s^{-1} and d^{-1} denotes the first decomposition stage. For the jth stage, where j is the highest resolution scale, the output signals are denoted by s^{-j} and d^{-j}. It is important to note that different WT's can be defined in terms of different sets of decomposition filters h and g.

For the Daubechies family of wavelets, the decomposition coefficients are computed via the use of circular convolutions, suitable for nonsymmetric decomposition filters. For the CH and BL families of wavelets, the decomposition filters are symmetric, and the signal is mirror extended before filtering. To describe the extracted signal frequency content, the decomposition coefficients are plotted in the time-frequency plane as illustrated in Fig. 1(a). In Fig. 1(a), f_s denotes the sampling frequency. The high-frequency content signal $d_0^{-1}, d_1^{-1}, d_2^{-1}, \ldots$ is plotted in the upper half-plane, while the low-frequency content signal $s_0^{-1}, s_1^{-1}, s_2^{-1}, \ldots$ is plotted in the lower half-plane. Due to the down sampling operation, each decomposition coefficient occupies two sampling periods. It is important to recognize that the time-frequency plot of Fig. 1 is only an approximation of the extracted time-frequency content. Clearly, no linear filter can extract signal information that is of finite duration in both the time and the frequency domains, since this would violate the uncertainty relation [17]. This point will be re-examined in the scalogram section.

For computing the two-stage WT, we re-compute the decomposition stage using the low-pass content signal $s_0^{-1}, s_1^{-1}, s_2^{-1}, \ldots$ as the new input. For the second-stage, the extracted time-frequency content is shown in Fig. 1(b) where only the lower-half of the time-frequency plane is affected by the second decomposition phase. It is clear that each decomposition phase uses half as many input coefficients as the previous stage. In terms of the time-frequency content extracted, the time-spread of each stage is double the spread of its previous stage, whereas the frequency-spread of each stage is half the spread of its previous stage. This is demonstrated in Fig. 1(a) and (b). For the third stage, the decomposition phase is recomputed for the second stage low-pass signal: $s_0^{-2}, s_1^{-2}, s_2^{-2}, \ldots$. Similarly, as long as the number of low-pass signal samples is comparable to the size of the decomposition filters, the procedure is repeated. For the reconstruction stage of the algorithm, first, the decomposition phase signals s^{-1} and d^{-1} are up-sampled by two. The up-sampled signals are then convolved with the appropriate reconstruction filters, and added to reproduce x. For two-stages, s^{-2} and d^{-2} are used to reconstruct s^{-1}. Then, s^{-1} and d^{-1} are used to reconstruct x. Similarly, the procedure is repeated for multiple stages.

B. Multiresolution Analysis

The WT is also used to analyze signals at different resolution levels. The process of analyzing signals at different resolution levels (scales) is known as multiresolution analysis. In this

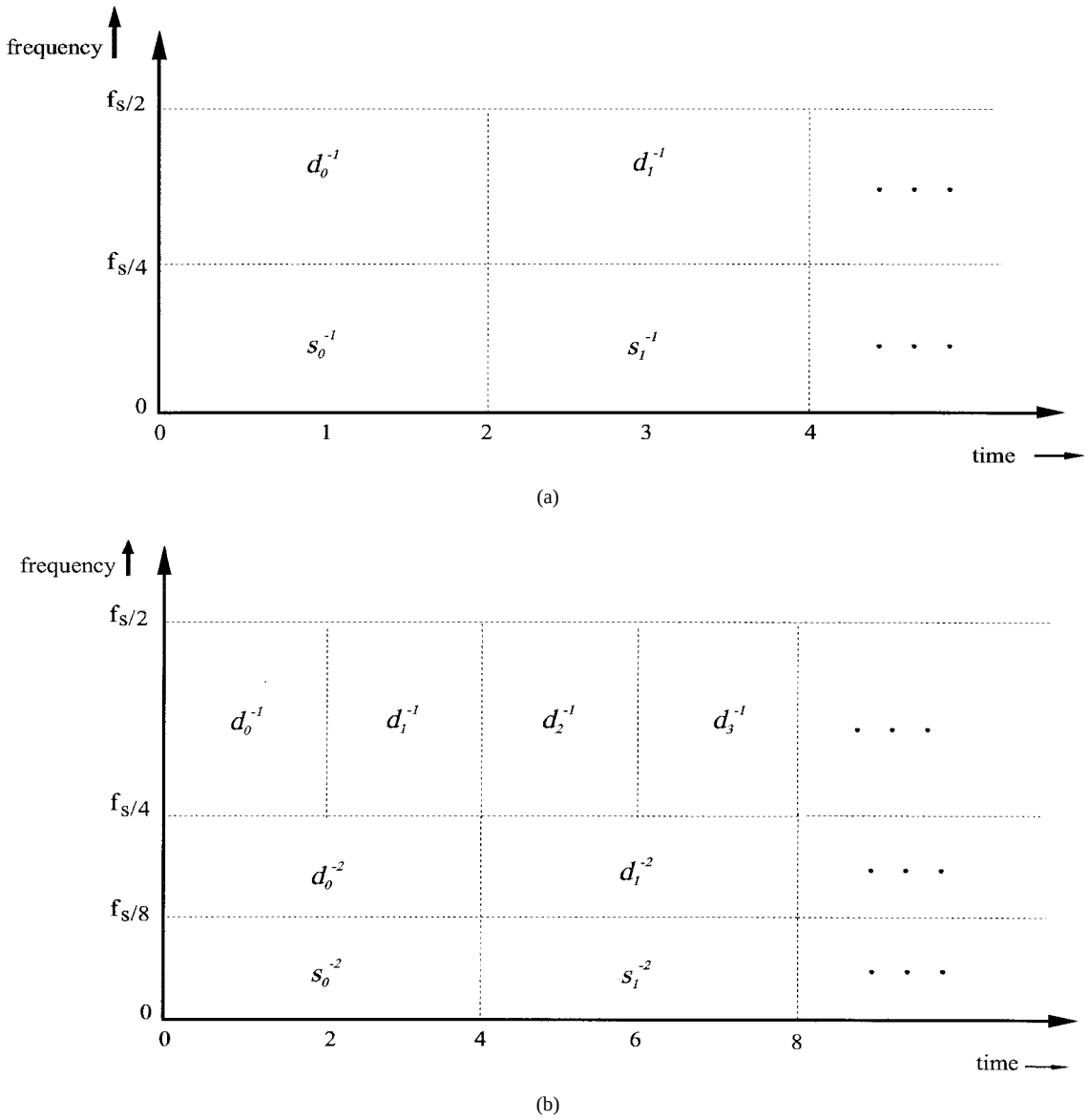

Fig. 1. Time-scale distribution of the WT decomposition phase outputs: (a) a single-stage WT and (b) a two-stage WT.

section, we briefly outline how the output coefficients from each stage of the WT can be used to construct functional approximations to the original signal. We limit our discussion to the spline based wavelets, CH and the BL. As before, we begin with the decomposition phase of the first stage of the WT. Given the signal samples $x_0, x_1, x_2, \ldots$, the corresponding continuous time signal is given by

$$f^0(t) = \sum_k x_k \phi(t-k) \tag{1}$$

where $\phi(.)$ is called a scaling function. In writing (1), we assume that the signal samples are weighted averages of the continuous time signal. The scaling function is the time domain representation of the low-pass filter at the zeroth stage. For the CH and BL families of WT's, the scaling functions are the familiar spline functions [14] where the original signal is approximated by a piecewise-polynomial representation.

After applying the decomposition phase, the signal approximation is decomposed in two separate signals

$$f^0(t) = \sqrt{2} \sum_k s_k^{-1} \phi(2t-k) + \sqrt{2} \sum_k d_k^{-1} \psi(2t-k) \tag{2}$$

where $\psi(.)$ denotes the wavelet function. The scaled wavelet function $\sqrt{2}\psi(2t)$ represents the time-domain representation of the highpass filter at the first stage. To recognize the purpose of the wavelet function, we rewrite (2) as

$$f^0(t) - f^{-1}(t) = \sqrt{2} \sum_k d_k^{-1} \psi(2t-k) \tag{3}$$

where $f^{-1}(.)$ is formally defined by

$$f^{-1}(t) \equiv \sqrt{2} \sum_k s_k^{-1} \phi(2t-k). \tag{4}$$

In (4), $f^{-1}(.)$ denotes the new signal approximation at the first stage. Here, is an approximation of the original signal $f^0(.)$

using spline functions $\phi(.)$ centered about the even integers. Thus, the $f^{-1}(.)$ approximation is ideal whenever the signal is nice and smooth, and well approximated by piecewise-polynomials over twice the support of the splines used for the $f^{0}(.)$ approximation. For rapidly changing signals, like MUAP's, the $f^{-1}(.)$ approximation is significantly worse than the $f^{0}(.)$ approximation, and the approximation difference $f^{0}(.) - f^{-1}(.)$ is captured in the wavelet expansion (3). Thus, the highpass filter coefficients d^{-j} capture the rapidly changing features of the signal. When such features are captured in an early stage $(j = 1, 2)$, the location of such features can be determined with accuracy (see Fig. 1).

C. Scalogram

In this section scalograms are introduced for analyzing nonstationary signals. First, the scalogram is defined in terms of the WT. Then, we briefly describe how it can be used to analyze stochastic processes and outline how the scalogram results depend on the wavelet used for computing the WT. The (discrete) scalogram is defined in terms of the square of the decomposition phase coefficients [18]. For a single-stage WT, the scalogram is identical to the time-frequency plot of Fig. 1(a), but with each of the coefficients squared. Similarly, for a two-stage WT, the scalogram is identical to the time frequency plot of Fig. 1(b), with each coefficient squared. Scalograms are used in analyzing nonstationary signals. For our purposes, we view a MUAP signal as a sample function of a stochastic process. Then, the sample scalogram is computed for each MUAP. Each coefficient in the sample scalogram represents a random variable. The scalogram captures the smoothness of the MUAP in the lower scale coefficients (at reduced time resolution), while the nonsmooth, transient variations are captured in the higher scale coefficients (at higher time resolution). An estimate of the MUAP scalogram for each subject is computed by ensemble averaging the sample scalograms of 20 aligned MUAP's as will be explained in the following section.

For any given ensemble of signals, the estimated scalograms are a function of the wavelet that was used to compute them. In this study, four different wavelets were investigated: DAU4, DAU20, CH, and BL. The DAU4 and DAU20 can be represented exactly using a finite number of coefficients (FIR), unlike the CH and BL WT's that are only approximated using a finite number of coefficients (IIR). For the Daubechies family of wavelets, the DAU4 is defined in terms of only four coefficients, while the DAU20 is defined in terms of twenty coefficients. (For the values of low-pass coefficients for DAU4 and DAU20 refer to [13, Table VI.A] $N = 2$ and $N = 10$, respectively.) Since the DAU4 is affected by much fewer signal samples than the DAU20, it is clear that the DAU4 has a better time-resolution than the DAU20. On the other hand, by design, the DAU20 provides a much better approximation to the ideal low-pass/high-pass decomposition filters. This tradeoff between the time and scale, resolutions obey the uncertainty principle. For rapidly changing signals, like MUAP's, in the region of the main spike time-resolution is preferred to scale-resolution. From the multiresolution analysis perspective at the power scales, the CH and BL WT's provide the familiar piecewise-polynomial approximation to the signal [16], [18]. Piecewise polynomial wavelets are important because they allow us to better characterize the wavelet coefficients in the time domain. The wavelet coefficients describe how the sharp signal discontinuities translate into derivative discontinuities at different scales. No such intuitive time domain characterization is possible for the Daubechies wavelets that are very irregular. (For the CH and BL wavelet coefficients refer to [14, Appendix A] and [15, Appendix A], respectively. For reconstruction, for DAU4, DAU20, and BL, the relationships between the high-pass and low-pass coefficients as described in [13, Fig. 5.10 and Fig. 5.11] were used).

III. Experimental Procedure

The EMG signal was acquired from the biceps brachii muscle using a concentric needle electrode. The signal was band-pass filtered at 3 Hz to 10 kHz and sampled at 20 kHz for 5 s with 12-b resolution. The signal was then lowpass filtered at 8 kHz. An automatic parametric pattern recognition (PPR) algorithm was used to identify MUAP's recorded from the same motor unit [19], [20]. The PPR algorithm is given in more detail in Appendix A. The PPR algorithm was designed to identify at least three MUAP's, which belong to the same group. The classification was based on the MUAP features: phases, amplitude, spike duration, and duration examined in sequence. MUAP's belonging to the same group were averaged to obtain the averaged MUAP envelope, simply referred to as MUAP. A MUAP waveform consisted of 512 points (25.6 ms), having the maximum peak in the region of 200 points (10 ms). For each MUAP, the sample mean was computed for the whole signal epoch. The sample mean was then subtracted from the MUAP waveform, resulting in a zero-mean signal epoch [21]. A total of 20 MUAP's were recorded from each muscle for analysis. The MUAP's were analyzed in the time, frequency, and time-frequency domains. For time domain analysis, the following MUAP features were extracted as described in Appendix A: 1) duration, 2) spike duration, 3) amplitude, 4) area, 5) spike area, 6) phases, and 7) turns (see Fig. 2). For frequency domain analysis the following measures were derived from the autoregressive (AR) power spectrum as described in Appendix A: 1) spectral moments of order zero, one, and two, 2) median frequency, 3) maximum frequency, 4) bandwidth, and 5) quality factor.

IV. Material

Neuromuscular diseases are a group of disorders whose main characteristic is that they cause muscular weakness and/or muscle tissue wasting. These disorders affect the motor nuclei of the cranial nerves, the anterior horn cells of the spinal cord, the nerve roots and spinal nerves, the peripheral nerves, the neuromuscular junction, and the muscle itself. In this study, the following three groups of subjects were investigated: 12 normal (NOR), 15 motor neuron disease (MND), and 13 myopathy (MYO). The time domain and frequency domain features for the three groups are given in Table I. The same

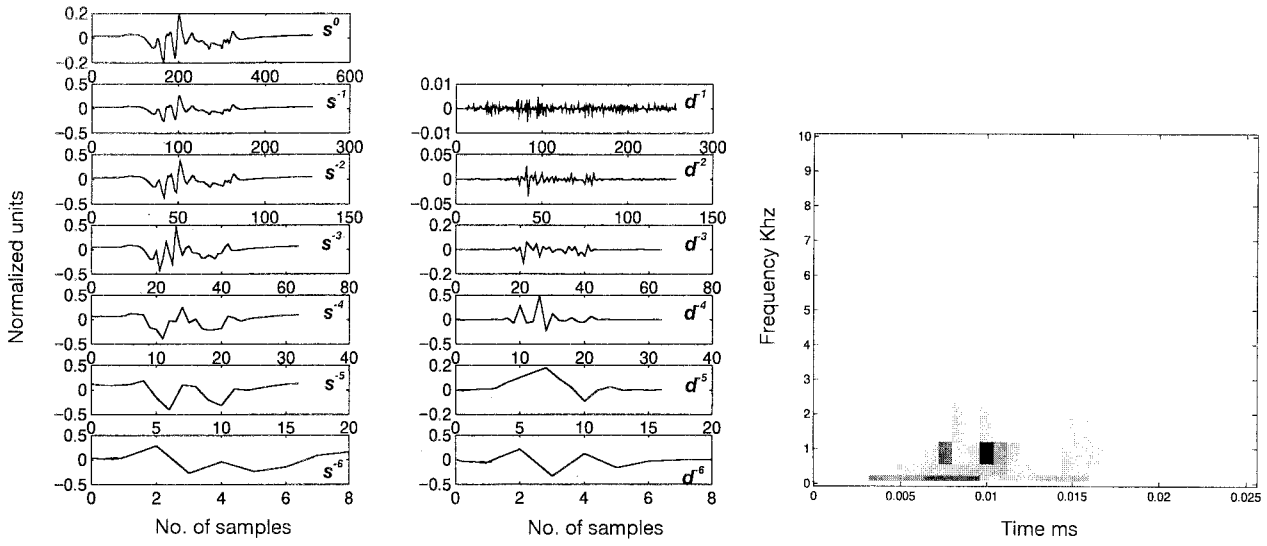

(a) (b) (c)

Fig. 2. Illustration of MUAP signal decomposition using the BL wavelet: (a) coarse waveforms $(s^0, \ldots, s^{-6})$, (b) detail waveforms $(d^{-1}, \ldots, d^{-6})$, and (c) MUAP scalogram. (The MUAP waveform was normalized for unit energy). (For the scalogram plot, black = maximum energy and white = minimum energy.)

TABLE I
MEAN (mn) AND STANDARD DEVIATION (sd) OF TIME DOMAIN AND FREQUENCY DOMAIN MUAP PARAMETERS FOR THE NOR, MND, AND MYO GROUPS

Time domain														
	Duration ms		Spike Duration ms		Amplitude mV		Area mVms		Spike Area mVms		Phases		Turns	
	mn	sd	mn	sd	mn	sd	mn	sd	mn	sd	mn	sd	mn	sd
NOR	9.60	2.75	5.40	2.46	0.376	0.306	0.370	0.198	0.232	0.118	2.6	0.8	3.0	2.0
MND	13.42	3.86	6.86	4.09	0.614	0.426	0.832	0.590	0.520	0.369	4.0	1.8	4.7	2.5
MYO	7.15	2.34	4.21	1.83	0.314	0.250	0.234	0.193	0.163	0.132	2.7	1.0	3.1	1.2

Frequency domain														
	M_0^+ mV^2		M_1^+ $mV^2/s*10^3$		M_2^+ mV^2/s^2*10^6		Median frequency Hz		Maximum frequency Hz		Bandwidth Hz		Quality factor	
	mn	sd	mn	sd	mn	sd	mn	sd	mn	sd	mn	sd	mn	sd
NOR	20.71	15.02	15.34	23.06	24.52	51.95	413	285	215	278	525	432	0.47	0.57
MND	15.30	11.80	9.54	17.59	14.12	39.70	339	241	213	240	381	349	0.71	0.98
MYO	29.70	16.88	27.68	27.18	45.41	21.74	629	344	411	389	767	539	0.63	0.78

$^+$ M_0, M_1, and M_2 represent spectral moments of order 0, 1 and 2 respectively.

data were also used in the studies by Elia [3] and Pattichis [19], [20].

V. RESULTS

A total of 800 MUAP's were analyzed using the DAU4, DAU20, linear spline CH, and cubic spline BL wavelets. The software used for wavelet analysis was developed at the University of Texas at Austin, and the University of Cyprus. Each MUAP was represented with 512 samples, sampled at 20 kHz, making the total analysis epoch of 25.6 ms. For each MUAP, the sample mean was computed and then subtracted. Furthermore, each MUAP signal was normalized to be of unit energy. For nonstationary analysis, the ensemble of MUAP's for each subject also had to be aligned so that all the sampled MUAP's were on the same (estimated) time axis. To this end, the maximum positive peak from each MUAP was shifted to the 200th sample ($t = 10$ ms). Following the time scale plots of Fig. 1, the scalogram parameters are listed in Table II. As explained earlier, time-frequency resolution

TABLE II
SCALOGRAM PARAMETERS (ANALYSIS WINDOW: $N = 512$, $T = 50$ μs, Epoch = 25.6 ms)

	No. of Points	Frequency Hz	Time Resolution ms
d^1	256	5000-10000	0.1
d^2	128	2500-5000	0.2
d^3	64	1250-2500	0.4
d^4	32	625-1250	0.8
d^5	16	312.5-625	1.6
d^6	8	156.25-312.5	3.2
s^6	8	0-156.25	3.2

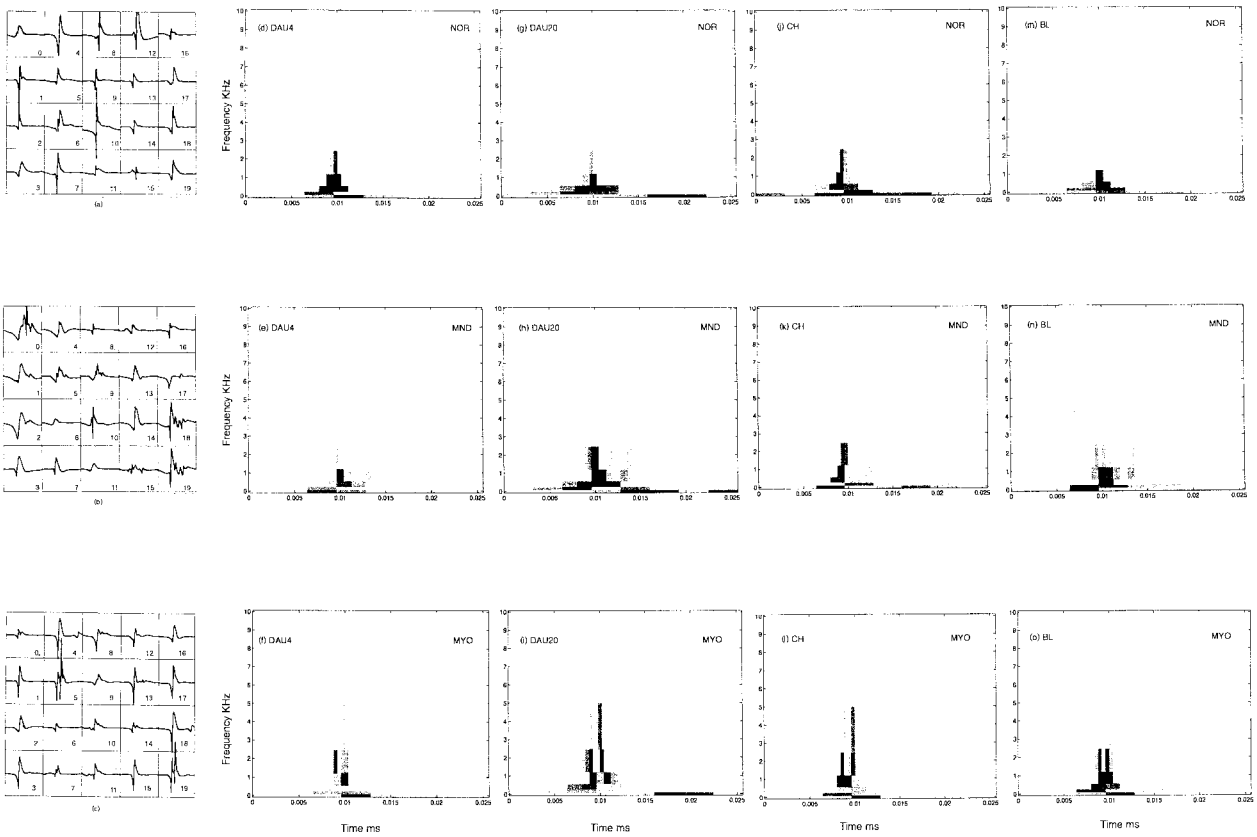

Fig. 3. Average scalograms of 20 MUAP's for NOR, MND, and MYO subjects. MUAP waveforms: (a) NOR, (b) MND, and (c) MYO. DAU4 scalograms for: (d) NOR, (e) MND, and (f) MYO. DAU20 scalograms for: (g) NOR, (h) MND, and (i) MYO. CHUI scalograms for: (j) NOR, (k) MND, and (l) MYO. BL scalograms for: (m) NOR, (n) MND and (o) MYO. (For the scalogram plot, black = maximum energy and white = minimum energy.)

is limited by the uncertainty principle. Thus, the scalogram parameters of Table II provide a general approximation for all wavelets. Wavelets with short time-domain spread have long frequency domain spread, whereas wavelets with long time-domain spread have short frequency domain spread.

A. An Example of MUAP Multiresolution Analysis, Fig. 2

For this example, the cubic spline BL wavelet was used. In Fig. 2, the signal approximation coefficients $s^0, s^{-1}, \ldots, s^{-6}$, and the detail coefficients $d^0, d^{-1}, \ldots, d^{-6}$, are plotted. The wave-shapes of the stage s^{-1}, s^{-2} and s^{-3} look very similar to the original coefficients s^0. However, as we move toward s^{-4}, the signal approximation decreases significantly, looking drastically different from s^0. Thus, significant signal features have been extracted at this stage. The extracted signal features, given as the difference signal $f^{-3}(.) - f^{-4}(.)$ are described by the wavelet coefficients d^{-4} as given in (3). In particular, the peaks in the d^{-4} coefficients correspond to the main spike locations of the MUAP. The location of the coefficient maxima corresponds to the location of the MUAP spikes, while the magnitude of each coefficient measures the abruptness in the spike. Fig. 3(c) illustrates the MUAP scalogram where

TABLE III
NORMALIZED PERCENTAGE MUAP WAVELET ENERGY DISTRIBUTION PER BAND FOR THE NOR, MND, AND MYO GROUPS

	DAU4			DAU20			CH			BL		
	NOR	MND	MYO	NOR	MNO	MYO	NOR	MND	MYO	NOR	MND	MYO
d^1	0.56	0.39	0.76	0.13	0.07	0.18	0.79	0.23	0.5	0.14	0.07	0.19
d^2	1.70	1.19	3.60	2.14	1.66	3.25	3.30	2.12	4.78	1.08	0.78	1.70
d^3	5.16	3.22	8.72	7.29	4.09	14.93	10.6	7.98	17.26	8.12	4.39	14.56
d^4	28.1	16.28	42.28	10.2	6.51	16.78	14.2	10.01	23.93	15.3	8.98	24.39
d^5	17.6	17.31	20.45	26.4	21.76	31.81	13.4	12.09	19.04	28.2	25.86	30.77
d^6	16.4	21.53	10.26	19.7	23.33	14.45	15.0	16.94	9.28	27.1	32.00	14.73
s^6	30.3	38.71	15.38	35.0	41.10	19.73	42.4	51.11	25.21	20.2	25.41	12.48

the magnitude square of the coefficients d^0, d^{-1}, ... d^{-6}, and s^{-6} shown in Fig. 2(a) and (b) are plotted (as given in Fig. 1 and Table II).

B. Average Scalograms of 20 MUAP's for NOR, MND, and MYO Subjects, Fig. 3

Next, we examine the average scalograms computed for the three types of subjects, using the four wavelets investigated. For each subject, an ensemble of 20 MUAP's is displayed on the left column of Fig. 3 starting from the top, with the ensemble for the NOR subject, followed by the ensembles for the MND and MYO subjects. Moving from left to right, the average scalograms for each ensemble for the DAU4, DAU20, CH, and BL wavelets are shown. For a particular subject type, the average scalograms from different wavelets exhibit certain similar characteristics. We next focus on these similarities, which remain consistent within each subject type, to help differentiate among the different types. The scalograms for the MND subject have longer time-domain spreads (compared to the scalograms for the NOR subject, see Fig. 3). On the other hand, the scalograms for the MYO subject have shorter time-dornain spreads compared to the scalograms for the NOR subjects.

Next, we interpret the different scalograms produced for the three subject types. The differences among these scalograms are due to the wavelet type used to derive them. For the three subject types, the DAU4 scalograms have the shortest time spread in each band. This is due to the fact that DAU4 uses the least number of finite impulse response coefficients, being only four. Furthermore, due to the small number of filter coefficients, the DAU4 scalograms detect the sharp MUAP spikes with high time-resolution (detected by coefficients d^{-1} and d^{-2}). On the contrary, the scalograms of DAU20, with 20 filter coefficients, have a longer time-domain spread. However, the DAU20 scalograms when compared to the DAU4 scalograms, have a shorter frequency-domain spread. The linear-spline CH scalograms show a large concentration of energy in the lowest band s^{-6}. From the multiresolution analysis perspective, this shows that the MUAP spikes can be well approximated by a piecewise linear approximation. On the contrary, the scalograms for the cubic spline BL wavelet are spread toward the upper frequency bands. From the multiresolution analysis perspective, this shows that the MUAP spikes exhibit strong discontinuities in the second (or higher) derivatives, which prohibits a good approximation by cubic splines. Thus, these derivative discontinuities are detected in the wavelet coefficients [as given in (3)].

For discriminating among subject types, we look at the statistical distribution of each scalogram coefficient separately. For orthogonal wavelets (and scaling functions), each coefficient describes an independent statistical measure. Both the Daubechies and the BL wavelets provide such measures. For semiorthogonal wavelets, statistical independence is maintained among the different scales, but not within translations of the basis function's of the same scale. This is true for the CH wavelet.

C. MUAP Wavelet Energy Distribution per Band for the NOR, MND, and MYO Groups, Table III

Table III tabulates the normalized MUAP wavelet energy distribution per band per group. It is shown that more than 77% of the energy is concentrated in d^{-4},\ d^{-5}, d^{-6}, and s^{-6}. Also, for all the wavelets, for the MND group there is a shift toward lower frequency bands, whereas for the MYO group there is a shift toward higher frequency bands when compared to the NOR group. These findings are in agreement with conventional frequency analysis as given in Table II for the median frequency parameter for the same group of subjects. The linear spline CH (semi-orthogonal) wavelet provides the best MUAP signal approximation by capturing most of the energy in the lowest resolution approximation coefficients. Kuskal–Wallis statistical analysis (nonparametric alternative to oneway ANOVA) of the normalized MUAP wavelet energy distribution per band for the NOR-MND, NOR-MYO, and MND-MYO groups was carried out. It was found that for d^{-4} and d^{-6} there are significant differences at $p < 0.05$ between the three groups for all the wavelets except for BL and CH. (The Kruskal–Wallis analysis was carried out using the SYSTAT package [22]).

D. Neural Network Classification of WT Coefficients, Table IV

Artificial neural network (ANN) models were developed for the classification of WT coefficients, into three groups: NOR, MND, and MYO. Since most of the MUAP energy is concentrated in the lower four bands d^{-4}, d^{-5}, d^{-6}, and s^{-4}, four coefficients from each of these bands in the region of the MUAP main spike were extracted for the neural network classification. These coefficients carry on average more than

TABLE IV
DIAGNOSTIC PERFORMANCE OF TIME DOMAIN, FREQUENCY DOMAIN, AND WAVELET COEFFICIENTS DAU4, DAU20, CH, AND BL FEATURE SETS USING THE BP, RBF, AND SOFM NEURAL NETWORKS. THE MEAN AND STANDARD DEVIATION OF THE DIAGNOSTIC YIELD, DY%, IS GIVEN FOR THE EVALUATION SET AFTER BOOTSTRAPPING THE AVAILABLE DATA FOR FIVE DIFFERENT SETS OF SUBJECTS

Feature set	n+	BP DY%	RBF DY%	SOFM DY%	Average DY%
Time domain	7	81.2 ± 11.8	72.5 ± 8.5	81.2 ± 5.5	78.3 ± 8.6
Frequency domain	5	63.7 ± 2.5	60.0 ± 6.3	63.7 ± 10.1	62.5 ± 6.3
Wavelet DAU4	16	68.7 ± 5.5	60.0 ± 5.0	70.0 ± 6.1	66.2 ± 5.5
Wavelet DAU20	16	57.5 ± 8.3	55.0 ± 4.6	66.2 ± 6.3	59.6 ± 6.4
Wavelet CH	16	65.0 ± 6.3	56.2 ± 11.8	68.7 ± 3.9	63.3 ± 7.3
Wavelet BL	16	65.0 ± 10.1	66.2 ± 8.5	66.2 ± 5.0	65.8 ± 7.9

+feature set vector size representing the average of 20 MUAPs per subject.

65% of the total MUAP energy and were the following: d_{10}^{-4} to d_{13}^{-4}, d_5^{-5} to d_8^{-5}, and d_1^{-6} to d_4^{-6}. For s_4^{-6} for each coefficient the mean for 20 MUAP's was computed for each subject. Three different neural networks were investigated, the back-propagation (BP) [23], the radial-basis function network (RBF) [24], and the self-organizing feature map (SOFM) [25]. These algorithms were implemented as given in the MATLAB neural network toolbox [26].

For training the ANN classifiers, a total of 480 MUAP's obtained from 24 subjects, eight NOR, eight MYO, and eight MND, were used, whereas for evaluation, a total of 320 MUAP's, obtained from 16 subjects, four NOR, five MYO, and seven MND were used. The system was trained and evaluated using five different bootstrap sets where in each set 24 different subjects were selected at random for training and 16 different subjects for evaluation as described above. Table IV tabulates the mean and standard deviation of the percentage of correct classifications, i.e., DY for the five bootstrap sets for each classifier for the evaluation set. In addition, the ANN classification performance of the mean time domain parameters (duration, spike duration, amplitude, area, spike area, number of phases, and number of turns) and frequency domain parameters (spectral moments of order zero, one, and two, median frequency, and quality factor) are tabulated. The feature vector representing each subject was computed by averaging the parameters of 20 MUAP's for both the time and frequency domain measures.

As shown in the average DY column of Table IV, the highest yield was obtained for the time domain parameters, followed by the DAU4, BL, and CH wavelet coefficients. The frequency domain parameters gave even lower DY, followed by the DAU20 wavelet coefficients.

VI. DISCUSSION

Quantitative analysis in clinical EMG is very desirable because it allows a more standardized, sensitive and specific evaluation of the neurophysiological findings. With the development of computer-aided EMG equipment different methodologies in the time domain and frequency domain have been followed for quantitative analysis. In this study, the usefulness of the WT that provides a linear two dimensional time-scale representation of nonstationary signals is investigated for describing MUAP morphology. For the orthogonal WT, each scalogram coefficient provides an independent statistical measure and it is shown that MUAP signals can be well represented using a small number of significant coefficients that are located around the main spike. High-frequency coefficients are highly localized in time and capture the location of MUAP spike changes whereas low-frequency coefficients provide lower time localization describing the average behavior of the signal. This multiscale analysis would not have been possible with the STFT, since the STFT uses a fixed size window. The DAU4 wavelet provides good time-resolution, capable of tracking the rapid changes in the MUAP's. The linear-spline CH wavelet provides the best signal approximation, capturing the average behavior of the MUAP's, as given by the energy content captured by the eight coefficients at the lowest frequency band.

WT energy distribution per band findings are in agreement with earlier frequency analysis studies that showed a displacement toward lower frequencies for neurogenic lesions, with the opposite being true for myogenic lesions [3]–[11]. Also, it is shown that the WT total energy at d^{-4} and d^{-6} (frequency bandwidth 156.25–312.5 Hz), with the exception of BL, was significantly, different between the NOR-MND, NOR-MYO, and MND-MYO groups.

The discriminative power of wavelet coefficients for the classification of MUAP's recorded from, NOR, MND, and MYO subjects was investigated using neural networks. Among the four wavelets studied, the best average DY was obtained for the DAU4 wavelet coefficients being 66.2%, followed by the BL, CH, and DAU20 wavelet coefficients with yields equal to 65.8%, 63.3%, and 59.6%, respectively. The time domain parameters, gave higher DY than the wavelet coefficients, being 78.3%. It is interesting to note that although the 16 wavelet coefficients used for neural network classification captured most of the energy of the MUAP signals (>65%), they gave lower DY than the time domain parameters which were empirically defined. A similar DY in the region of 78%–80%

for the time domain parameters was also obtained using neural network [19], [20], and genetics-based machine learning [27].

In a recent paper, we showed that MUAP time-domain and wavelet analysis can be combined into a modular neural network decision support system in order to improve the classification performance of individual features or classifiers [28]. More specifically, a decision making system was developed in [28] where BP, RBF, and SOFM classifiers were trained with time domain, frequency domain, AR coefficients, cepstral coefficients and DAU4, DAU20, CH, and BL wavelet coefficients (as described in Section V-E). (It is noted that the average DY's for the AR, and cepstral coefficients feature sets were 63% and 51.2%, respectively [28].) The 24 output results of the eight feature sets applied to the three classifiers were combined using majority voting, i.e., a subject was assigned to the class with the maximum number of votes. The DY achieved with the combination of the 24 classification results, was 82.5%. This DY was higher than the DY of the best feature set from the best classifier, which was 81.2% for the time domain parameters and the SOFM and BP classifiers as given in Table IV.

In conclusion, wavelet analysis provides a new way in describing MUAP morphology in the time-frequency plane. This method allows for the fast extraction of localized frequency components of MUAP's that may prove to be valuable in the early and accurate diagnosis of neuromuscular disorders. Future work will integrate wavelet analysis to a hybrid diagnostic system for neuromuscular diseases where EMG, muscle biopsy, biochemical and molecular genetic findings, and clinical data are combined to provide a diagnosis [29]. Furthermore, the interpretation of wavelet analysis coefficient changes in relation to muscle pathophysiology can be investigated. More specifically, the following factors that have been proven to affect conventional spectral analysis can be studied [9]: MUAP propagation velocity, velocity dispersion, size of innervation zone, number of fibers in the motor unit, and electrode recording site.

APPENDIX
TIME DOMAIN AND FREQUENCY DOMAIN MUAP PARAMETERS

A. Time Domain Parameters [19], [20]

For each potential the following seven parameters were measured.

1) *Duration (Dur):* MUAP beginning and ending are identified by sliding a measuring window of length 3 ms and width ± 10 μV.
2) *Spike Duration (SpDur):* Measured from the first to the last positive spike.
3) *Amplitude (Amp):* Difference between the minimum positive peak and the maximum negative peaks.
4) *Area:* Sum of the rectified MUAP integrated over the duration measure.
5) *Spike Area (SpArea):* Sum of the rectified MUAP integrated over the spike duration.
6) *Phases (Ph):* Number of baseline crossings that exceed 25 μV plus one.
7) *Turns (T):* Number of positive and negative peaks separated from the proceeding and following peak by 25 μV.

B. Spectral Analysis Parameters [3]

For each MUAP, the AR coefficients a_k were calculated using the modified covariance algorithm as given in [21]. The AR power spectrum of each MUAP was estimated, and it was normalized with its maximum power value. The following parameters were computed from the AR power spectrum curve.

1) Moments of order zero, one, and two: A moment M_j of order j was computed as given in [9]:

$$M_j = \frac{2}{(2\pi)^{j+1}} \sum_{n=0}^{N-1} f(n)^j \mathrm{PAR}(f(n)).$$

2) Median frequency (FMED) is the frequency at which the power spectrum is divided into two regions with equal power.
3) Maximum frequency F_0 is the frequency with the maximum power.
4) Quality factor (Q) is the ratio of the dominant peak frequency F_0 divided by the bandwidth (BW) and is expressed as: $Q = F_0/BW$.
5) Bandwidth (BW) is the difference of frequencies at the upper (F_2) and lower $(F_1) - 3$ dB points of the power spectrum and is given as: $BW = F_2 - F_1$.

ACKNOWLEDGMENT

The authors would like to express their sincere thanks to the anonymous reviewers for their constructive comments.

REFERENCES

[1] F. Buchthal, *An Introduction to Electromyography.* Copenhagen, Denmark: Gyldendal, 1957.
[2] E. Stalberg, S. Andreassen, B. Falck, H. Lang, A. Rosenfalck, and W. Trojaborg, "Quantitative analysis of individual motor unit potentials: A proposition for standardized terminology and criteria for measurement," *J. Clin. Neurophysiol.*, vol. 3, no. 4, pp. 313–348, 1986.
[3] A. Elias, "Autoregressive spectral modeling of motor unit action potentials," M.Sc. dissertation, Dept. Elec. Eng., Queen Mary and Westfield College, Univ. London, London, U.K., 1994.
[4] G. Pfeiffer and K. Kunze, "Frequency analysis and duration of motor unit potentials: Reliability and diagnostic usefulness," *Elect. Clin. Neurophrol.*, vol. 89, pp. 365–374, 1993.
[5] J. N. Walton, "The electromyograph in myopathy: Analysis with the audio frequency spectrometer," *J. Neural Neurosurg. Psych.*, vol. 15, pp. 219–226, 1952.
[6] J. Fex and C. E. T. Krakau, "Some experiences with Walton's frequency analysis of the electromyogram," *J. Neural, Neurosurg. Psych..*, vol. 20, pp. 178–184, 1957.
[7] E. Kaiser and I. Petersen, "Muscle action potentials studied by frequency analysis and duration measurement," *Acta Neural. Scand.*, vol. 41, pp. 213–236, 1965.
[8] J. Kopec and L. Hausmanowa-Petrusewicz, "Application of harmonic analysis to the electromyogram's evaluation," *Acta Physiol. Polonica*, vol. 17, pp. 597–608, 1966.
[9] L. Lindstrom and I. Petersen, "Power spectrum analysis of EMG signals and its application in computer-aided electromyography," in *Progress in Clinical Neurophysiology*, J. E. Desmed, Ed. Brussels, Belgium: Karger, 1983, vol. 10, pp. 1–51.
[10] S. Johansson, L. E. Larsson, and R. Ortengren, "An automated method for the frequency analysis of myoelectric signals evaluated by an inves-

tigation of the spectral changes following strong sustained contractions," *Med. Biol. Eng.*, vol. 8, pp. 257–264, 1970.
[11] L. E. Larsson, "On the relation between the EMG frequency spectrum and the duration of symptoms in lesions of the peripheral motor neuron," *Electroencephal. Clin. Neurophysiol*, vol. 38, pp. 69–78, 1975.
[12] C. S. Pattichis, M. S. Pattichis, and C. N. Schizas, "MUAP wavelet analysis," in *Proc. 18th Ann. Int. Conf. IEEE Eng. in Medicine and Biology*, Amsterdam, The Netherlands, 1996, paper 553.
[13] I. Daubechies, *Ten Lectures On Wavelets.* Philadelphia, PA: SIAM, 1992.
[14] K. Chui, *Wavelet Analysis and its Applications Volume—1: An Introduction to Wavelets.* San Diego, CA: Academic, 1992.
[15] S. G. Mallat, "A theory for multiresolution signal decomposition: The wavelet representation," *IEEE Trans. Pattern Anal. Machine Intell.*, vol. 11, pp. 674–693, July 1989.
[16] G. Strang and T. Nguyen, *Wavelets and Filter Banks.* Wellesley, MA: Wellesley-Cambridge Press, 1996.
[17] A. Papoulis, *Signal Analysis.* New York: McGraw Hill, 1977.
[18] O. Rioul and P. Flandrin, "Time-scale energy distributions: A general class extending wavelet transforms," *IEEE Trans. Acoust., Speech, Signal Processing*, vol. 40, pp. 1746–1757, July 1992.
[19] C. S. Pattichis, "Artificial neural networks in clinical electromyograpy," Ph.D. dissertation, Dept. Elect. Eng., Queen Mary and Westfield College, Univ. London, London, U.K., Mar. 1992.
[20] C. S. Pattichis, C. N. Schizas, and L. T. Middleton, "Neural network models in EMG diagnosis," *IEEE Trans. Biomed. Eng.*, vol. 42, pp. 486–496, May 1995.
[21] S. L. Marple, Jr., *Digital Spectral Analysis with Applications.* Englewood Cliffs, NJ: Prentice-Hall, 1987.
[22] L. Wilkinson, *SYSTAT: The System for Statistics.* Evanston, IL: SYSTAT, 1988.
[23] D. E. Rumelhart, G. E. Hinton, and R. J. Williams, "Learning representations by back propagating errors," *Nature*, vol. 323, pp. 533–536, 1986.
[24] D. S. Broomhead and D. Lowe, "Multivariable functional interpolation and adaptive networks," *Complex Syst.*, vol. 2, pp. 321–355, 1988.
[25] T. Kohonen, *Self-Organizing Maps*, Series in Information Sciences. Berlin, Germany: Springer-Verlag, 1995.
[26] H. Demuth and M. Beale, *Neural Network Toolbar User's Guide, to Use With MATLAB.* MA: The MathsWork, Inc. Natick, MA, 1994.
[27] C. S. Pattichis and C. N. Schizas, "Genetics-based machine learning for the assessment of certain neuromuscular disorders," *IEEE Trans. Neural Networks*, vol. 7, pp. 42–439, Feb. 1996.
[28] C. I. Christodoulou, C. S. Pattichis, and W. F. Fincham, "A modular neural network decision support system in EMG diagnosis," *J. Intell. Syst., Special Issue on Computational Intelligent Diagnostic Systems in Medicine*, vol. 8, no. 12, pp. 99–143, 1998.
[29] C. N. Schizas, C. S. Pattichis, and C. A. Bonsett, "Medical diagnostic systems: A case for neural networks," *Technol. Health Care*, vol. 2, p. 1, 1994.

Constantinos S. Pattichis (S'88–M'88) was born in Nicosia, Cyprus, on June 30, 1959. He received the B.Sc. degree in electrical engineering from the University of New Brunswick, Fredericton, N.B., Canada, in 1983, the M.Sc. degree in biomedical engineering from the University of Texas at Austin, in 1984, the S.Sc. degree in neurophysiology from the University of Newcastle upon Tyne, Newcastle upon Tyne, U.K, in 1988, and the Ph.D. degree in electronic engineering from the University of London, London, U.K, in 1992.

From 1985–1992, he was also working with the Cyprus Institute of Neurology and Genetics, Nicosia, Cyprus, where he is now a Visiting Senior Scientist. He is currently an Assistant Professor with the Department of Computer Science at the University of Cyprus. He is actively participating in a number of European projects related to medical imaging and health telematics. His current research interests include medical imaging, biosignal analysis, artificial neural networks, and genetic algorithms. He has published more than 50 refereed journal and conference papers in these areas.

Dr. Pattichis was the recipient of the 1994 European Community "Marie-Curie" Fellowship in image processing in histopathology. He has been involved in numerous professional society activities, including President of the Cyprus Association of Medical Physics and Biomedical Engineering, 1996–1998; President of the IEEE Cyprus Section, 1998–1999; General Co-Chairman, Medical and Biological Engineering and Computing Conference'98 (Medican'98) June 14–17, 1998.

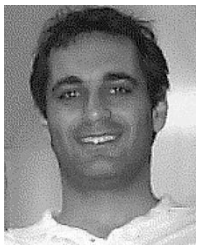

Marios S. Pattichis (S'90–A'95) was born in Nicosia in 1967. He received the B.S. (Hons.) degree in computer science and the B.A. (Hons.) degree in mathematics in 1991. He also received the M.Sc. and Ph.D. degrees in electrical engineering in 1993 and 1998, respectively, all from the University of Texas at Austin.

He is currently a Visiting Assistant Professor in the Department of Electrical and Computer Engineering and the Center for High-Performance Computing, at the University of New Mexico. His research interests are in the broad area of signal and image processing, with an emphasis on AM–FM transforms and their applications, his dissertation topic.

For his undergraduate studies, Dr. Pattichis received a scholarship from the Cyprus-America Scholarship program.